Iterative *in silico* identification of P-glycoprotein inhibitors

Lauren A. McCormick [1,2,3,*] & James W. McCormick[1,2,3,*], Chanyang Park[1,2,3], John G. Wise [1,2,3], and Pia D. Vogel[1,2]

[1]Department of Biological Sciences, the [2]Center for Drug Discovery, Design and Delivery, and the [3]Center for Scientific Computation, Southern Methodist University, Dallas, Texas

Corresponding author: Pia D. Vogel, pvogel@smu.edu

[*]Co-first authors: LA McCormick and JW McCormick.

Keywords: P-glycoprotein, P-gp, Molecular Docking, ABC Transporter, *in silico* screening, Drug Discovery, Multidrug resistance, cancer, chemotherapy resistance, Molecular Dynamics, virtual screening

ABSTRACT

Overexpression of the polyspecific efflux transporter, P-glycoprotein (P-gp, MDR1, *ABCB1*), is a major mechanism by which cancer cells acquire multidrug resistance (MDR), the resistance to diverse chemotherapeutic drugs. Inhibiting drug transport by P-gp can resensitize cancer cells to chemotherapy. However, there are no P-gp inhibitors available to patients. Clinically unsuccessful P-gp inhibitors tend to bind at the pump's transmembrane drug binding domains and are often P-gp transport substrates, resulting in lowered intracellular concentration of the drug and altered pharmacokinetics. In prior work, we used virtual-assisted drug discovery to identify novel P-gp inhibitors that target the pump's cytoplasmic nucleotide binding domains and showed that these domains are viable drug discovery targets. Here we develop an enhanced virtual-assisted pipeline that expands upon prior work by iteratively screening compounds against multiple regions and conformations of P-gp. This increased computational complexity is offset by custom Tanimoto chemical datasets which compress the initial docking library while maximizing chemical diversity. Molecules that were similar to resultant hits were subsequently retrieved and screened. We identified nine novel P-gp inhibitors that reverse MDR in two types of P-gp overexpressing human cancer cell lines, reflecting a 14% hit rate. Of these inhibitors, all were non-toxic to non-cancerous human cells, and six were not transport substrates of P-gp. Our novel P-gp inhibitors are chemically diverse and are good candidates for lead optimization. Our results demonstrate that the nucleotide binding domains of P-gp are an underused target in the effort to reverse P-gp-mediated multidrug resistance.

INTRODUCTION

Multidrug resistance (MDR) is a significant obstacle to the successful treatment of cancer [1]. Cancer cells often acquire MDR by overexpressing ATP-binding cassette (ABC) transporters as a mechanism to overcome chemotherapeutic treatment [2]. Among the most clinically relevant of ABC transporters is P-glycoprotein (P-gp, MDR1, *ABCB1*), a remarkably promiscuous enzyme that cancer cells overexpress to evade chemotherapy-mediated cell death [2, 3]. P-gp harnesses the power of ATP hydrolysis to pump toxic compounds, xenobiotics, and physiologically relevant substrates out of the cell. The pump's cytoplasmic nucleotide binding domains (NBDs) bind and hydrolyze ATP, and its membrane-embedded drug binding domains (DBDs) recognize and extrude substrates [4]. P-gp's substrate profile is incredibly diverse, ranging from small drug molecules to bulky and flexible amyloid β peptides [5]. Importantly, P-gp transports a host of structurally and chemically diverse chemotherapeutics. Inhibiting P-gp's efflux activity is therefore predicted to raise intracellular drug concentrations to therapeutic levels and thereby resensitize MDR cancers to chemotherapy [6-9].

Decades of work have yielded three generations of clinically unsuccessful P-gp inhibitors [10, 11] (Supplemental Table 1). First and second-generation inhibitors targeted P-gp with relatively low specificity [10, 11] and failed in clinical trials due to off-target toxicity. All first and second-generation P-gp inhibitors are thought to bind at the pump's transmembrane DBDs, and many were shown to be P-gp transport substrates [10, 12]. Third-generation inhibitors (tariquidar, zosuquidar, and their derivatives) targeted the DBDs of P-gp with a higher affinity than previous generations of compounds but still failed in clinical trials due to toxicity [13, 14]. It was initially thought that tariquidar and zosuquidar were not P-gp transport substrates, but later work has shown otherwise [15, 16].

To date, most or all of the clinically unsuccessful P-gp inhibitors are likely to bind to the pump's transmembrane DBDs. It can be hypothesized that this shared characteristic may be a significant contributor to why these drugs failed in clinical trials. A molecule that binds the DBDs is likely to be a P-gp transport substrate. Treatment with P-gp transport substrates inherently requires higher doses because the pump continuously ejects the drug from the cell. This likely lowers the drug's inhibitory effect and only lasts while the inhibitor resides within the DBDs. Recent work on tariquidar and zosuquidar [16] has emphasized the difficulty of finding a DBD-binding inhibitor that is not also a P-gp transport substrate. As an additional complication, P-gp's hydrophobic DBDs are so large and flexible that transport substrates may take multiple pathways through the domains [17]. DBD-binding inhibitors often require the binding of several inhibitor molecules in order to inhibit the P-gp transport cycle. This, in turn, raises the required dose of inhibitor for successful treatment of patients [16] and likely leads to the adverse side effects observed in previous trials. Combined, these observations strongly indicate that the drug binding domains of P-glycoprotein are no longer promising targets for the design of clinically effective P-gp inhibitors. However, P-gp's nucleotide binding domains (NBDs) remain promising targets for the design of new P-gp inhibitors.

In previous studies, our group identified novel P-gp inhibitors using a virtual-assisted drug discovery program that targeted the P-glycoprotein's nucleotide binding domains. Our early screens successfully identified three inhibitors that reverse MDR in human cancer cells with a 7% hit rate [6, 7]. A fourth compound was identified that likely interacts with the nucleotide binding sites in biochemical and biophysical studies using isolated P-gp in vitro, but likely is not able to enter cells due to unfavorable negative charge at neutral pH (6). In this present study, we deployed an enhanced screening method to identify additional, novel P-gp inhibitors for lead optimization and testing. Virtual screens were expanded to incorporate the dynamic range of P-gp conformational transitions. Additionally, cell-based assays were extended to include robust assessments of inherent toxicity, cell line specificity, and potential transport by P-gp. Using this approach, we identified 9 novel P-gp inhibitors that reverse multidrug resistance in two types of P-gp overexpressing human cancer cell lines, which reflects a 14% hit rate. These nine novel inhibitors were non-toxic to non-cancerous human cells, and

six were shown to not be transport substrates of P-gp itself. These novel P-gp inhibitors are deemed to be good candidates for further lead optimization and testing. Our work reinforces the idea that P-gp's nucleotide binding domains are promising targets in the fight against multidrug resistance in cancer. This 'enhanced screening' approach can be adapted for drug discovery screens that target other clinically relevant ABC transporters such as the breast cancer resistance protein (BCRP, *ABCG2*) or Msba from *E. coli.*

METHODS

Receptor Generation for Virtual Screens against Human P-gp

A putative catalytic cycle of P-glycoprotein (P-gp, MDR1, *ABCB1*) was simulated using Targeted Molecular Dynamics (TMD) simulations with NAMD as described in [17, 18]. From these TMD simulations, we produced ten distinct conformations of P-gp based upon crystal structures of P-gp homologues: an approximate 4KSB position, 3B5X position, two 3B5Z positions, two 2HYD positions, and two positions between 4KSB and 3B5X named the "Transition" position (Supplemental Figure 1). Three structures (4KSB_DBD, Transition_DBD, and 3B5X_DBD) (Supplemental Figure 1, Boxes A-C) were used for docking against the drug binding domains (DBD), and five (3B5Z_NBD_1, 3B5Z_NBD_2, 2HYD_NBD_1, 2HYD_NBD_2 and Transition NBD) were used for docking against the nucleotide binding domains (NBD) (Supplemental Figure 1, Boxes D-F). The NBD search areas shown in Supplemental Figure 1D-F were divided into two separate dock boxes, each targeting the respective individual NBD. Receptor files were prepared as PDBQTs for docking using AutoDock Tools [19].

Ligand Selection and Preparation for Docking

Compounds were taken from the ZINC12 Clean Drug-Like Subset of 13,195,609 molecules (31). Molinspiration (*mib)* software was used to calculate logP, polar surface area, molecular weight, number of hydrogen-bond donors and acceptors and number of rotatable bonds for each ligand [20]. To predict the aqueous solubility of our experimental compounds, the AMSOL program was used to calculate polar and apolar desolvation energies [21]. The criteria for ligand selection conformed to Lipinski's rule of 5 for characteristics of drug-like or therapeutic molecules: (1) a molecular weight less than 500 and greater than 150 Daltons; (2) an octanol-water partition coefficient (log P) less than 5; (3) a topological polar surface area less than 150 $Å^2$; (4) less than 5 hydrogen donors; and (5) less than 10 hydrogen acceptors.

The dataset used to guide the purchase of compounds SMU 58-68 was obtained from a pre-calculated 90% Tanimoto cutoff set containing 123,510 "Clean Drug-Like Compounds" from the $Zinc^{12}$ database [22]. Ligands were obtained in mol2 file format at a pH of 7. We found that this subset was not structurally diverse, especially in molecular weight, and therefore only 10 compounds were purchased from it. For compounds SMU 68-124, we generated a custom 95% Tanimoto set from the ZINC Clean Drug-Like Subset using cactvs (http://www.xemistry.com/)

and SUBSET (https://cactus.nci.nih.gov/subset/); this resulted in a final dataset of 158,000 diverse molecules. The mol2 files from the ZINC database corresponding to the 158,000 compounds were converted to PDBQT format using Open Babel [23]. Open Babel 2.3.2 was used for the Zinc12 90% Tanimoto dataset and Open Babel 2.4.0 was used for the custom 95% Tanimoto dataset.

Ligand Docking and Iterative Screening with *Autodock Vina*

AutoDock Vina was used to dock each molecule against each target shown with an exhaustiveness of 128 (default exhaustiveness is set at 8), totaling over 4.2 million individual docking experiments (Supplemental Figure 1) [24]. The resultant ligand docking poses were ranked by predicted affinities/binding energies. Examples of ligand docking locations are shown in Supplemental Figure 2. All docking calculations were performed on the High-Performance Computing Facilities at SMU using the ManeFrame computing cluster. Docking results were downloaded to a Linux workstation, where bash scripts were used to extract and organize the individual files. For each ligand-target combination, the docking pose with the best predicted binding energy (kcal/mol) was extracted and used to calculate an estimated equilibrium constant of dissociation (estimated K_d). For concise evaluation of each ligand, the binding energy for each receptor-ligand pair was combined with the ligand molecular weight, logP, apolar desolvation (kcal/mol), polar desolvation (kcal/mol), H-bond donors, H-bond acceptors, net charge, topological polar surface area (TPSA), rotatable bonds, and simplified molecular-input line-entry system (SMILES string). The R language for statistical computing and graphics was used for manipulation and analysis of the combined data. To identify ligands that might preferentially bind to the NBDs of P-gp instead of the DBDs, we looked for molecules with a high estimated K_D NBD : estimated K_D DBD ratio. The predicted ratios for the top hits identified in this study are shown in Supplemental Table 4.

The PDBQT output files from *Autodock Vina* were converted into PDB file format compatible with Visual Molecular Dynamics (VMD), a PNG picture of the ligand was generated and the log files of the ligand docking were organized based on the receptor [24, 25]. The top 100 ligands with the best ratio of DBD/NBD predicted affinity (i.e. preferential docking to the nucleotide binding domains versus the drug binding domain) were used in ZINC to return molecules with 99-70% similarity. This produced a second dataset of ~100 - 10,000 molecules per top ligand which was docked and analyzed in the same way as the first set.

Property prediction and selection

The top 100 ligands against each target were subjected to property prediction using the Online Chemical Database (OCHEM) [26]. Compounds that passed certain filtering requirements (e.g. good ratio of binding to nucleotide binding domain over drug binding domain affinity) were loaded into OCHEM as a single SDF (structure-data file) containing all molecules as SMILES

(simplified molecular-input line-entry system) strings. OCHEM processing of ligand SMILES produced predictions for logP and Solubility, Environmental toxicity, Ames test, CYP3A4 inhibition, CYP2D6 inhibition, CYP2C19 inhibition, CYP2C9 inhibition, CYP1A2 inhibition, Melting Point best (Estate), Pyrolysis OEstate submodel, Water solubility (GSE) based on logP and Melting Point, ALOGPS 2.1 logS, ALOGPS 2.1 logP, DMSO solubility, and any known toxic effects from literature. Along with the specific docking location to the receptor as visualized in VMD, the structural, chemical, and docking information was used to select ligands for purchase and subsequent testing.

Testing of Experimental Compounds in Cell Culture

Culture of the DU145, DU145-TXR, and HFL1 cell lines was performed as described in [7]. Culture of the A2780 and A2780-ADR cell lines was performed as described in [8]. MTT assays were performed as described in [7] with minor modifications. LC-MS/MS accumulation assays were performed as described in [8] with some modifications. DU145-TXR cells were exposed to 500 nmol/L PTX, a dosage that has been shown to result in greater than 85% survival of the multidrug-resistant DU145-TXR cell line, and less than 10% survival of the chemotherapy-sensitive DU145 parental cell line [7]. Compounds 56 through 98 were pre-screened using Rezasurin cell viability assays: cells were incubated with 15 µM compound with or without 500 nM PTX for 48 hours, after which cell survival was assessed similar to [27]. Data represent the mean of two separate experiments, with n = 3 per experiment (n = 6 total) (Supplemental Table 6). The top performing compounds from this initial screen were re-tested with MTT viability assays against DU145-TXR cells, as described below.

Cell lines and cell culture

The chemotherapeutic sensitive DU145 human prostate cancer cells and the multidrug resistant sub-line, DU145-TXR, were generous gifts from Dr. Evan Keller (University of Michigan, Ann Arbor, MI) [28]. The MDR, P-gp overexpressing DU145-TXR cells were maintained under positive selection pressure by supplementing complete medium with 10 nM paclitaxel (Acros Organics, NJ). In addition to the aforementioned cell lines, the chemotherapeutic sensitive A2780 ovarian cancer cells (93112519, Sigma) and the multidrug resistant A2780-ADR (93112520, Sigma) were maintained in complete RPMI media consisting of RPMI-1640 with L-glutamine, 10% fetal bovine serum (FBS; Corning), 100 U/mL penicillin and 100 µg/mL streptomycin in a humidified incubator at 37°C and 5% CO2. The MDR, P-gp overexpressing A2780-ADR cell line was maintained under positive selection pressure by supplementing complete medium with 100 nM doxorubicin (Fisher Scientific, NJ). The non-cancerous HFL1 (human lung fibroblast) cell line was maintained in complete F12K media consisting of F12K with 10% fetal bovine serum, 100 U/mL penicillin, and 100 µg/mL streptomycin (Gibco). Flasks

and 96 well plates that were used with the non-cancerous line HFL1 were pre-treated with 0.01 mg / ml Collagen Type 1 (Gibco) and rinsed with PBS (Fisher).

MTT cell viability assays

MTT assays measure the reduction of yellow, water soluble 3-(4,5-dimethylthiazol-2-yl)-2,5-diphenyltetrazolium bromide (MTT) to blue, insoluble formazan crystals by cellular reductase processes in living cells [29]. Cells were trypsinized from monolayers and seeded in complete medium in 96 well plates. Cancerous cell lines (DU145, DU145-TXR, A2780, A2780-ADR) were seeded at 3,000 cells per well in complete RPMI medium. The non-cancerous HFL1 line was seeded at 4,000 cells per well in complete F12K medium, in collagen-treated plates (Collagen Type 1, Gibco). Cells were incubated with experimental compounds for 48 hours at 37 °C and 5% CO_2 in a humidified incubator. At 48 hours, MTT was added (20 µL/well of 5 mg/mL MTT in PBS) to each well. After incubation for 4 hours, the media was removed, and the formazan crystals were dissolved in 100 µL DMSO per well. Plates containing the semi-adherent A2780 or A2780-ADR lines were spun at 1400 rpm for 3 minutes prior to aspiration of media, and the addition of DMSO. Plates were shaken for 10 minutes at 500 rpm on an Orbital shaker (LabDoctor from MidSci, St Louis, MO). The absorbance was measured at 570 nm using a Bio-Tek Cytation 5 (Bio-Tek, Winooski, VT). The measured absorbance value was correlated with the number of metabolically active cells in that well. The percent of cell viability was calculated using the following equation:

$$\%\,Viability = 100 \times \frac{absorbance\ of\ experimental\ cells - absorbance\ of\ media}{absorbance\ of\ DMSO\ treated\ cells - absorbance\ of\ media}$$

For DU145-TXR, DU145, HFL1 and A2780 cells - data are the mean ± one standard deviation, n = 8 samples per compound, from at least two independent trials per compound. The semi-adherent A2780-ADR cells exhibited a much higher variability in MTT assays, necessitating a larger sample size. For A2780-ADR cells, data are the mean ± one standard deviation with n = 12 samples per compound, from at least two independent trials per compound.

Cell culture for LC-MS/MS intracellular accumulation assays

DU145-TXR cells were seeded at 350,000 cells per well in 6-well plates in complete RPMI medium. After 48 hours, the media was replaced with fresh media, and cells were treated with 5 µM of experimental compound with or without 500 nM Tariquidar (TQR). Experiments were performed in triplicate with two independent trials per compound, n = 6 total, or three independent trials per compound, n = 9 total. The P-gp substrate, Daunorubicin (DAU), was included in each biological replicate as a qualitative positive control – DAU is red, so the TQR-inhibited sample with DAU turns visibly red to the naked eye. A full sample of DAU was also prepared for quantitative analysis. After a 2.5 hour incubation with the respective treatment,

cells were trypsinized (0.05% Trypsin-EDTA, Gibco, ice-cold), scraped with a cell scraper, and spun at 2400 rpm. Media was removed with a glass vacuum aspirator. Cells were re-suspended and washed in 2mL of ice-cold Hank's Balanced Salt Solution (HBSS, Gibco), and spun again at 2400 rpm. Cell lysates were diluted in 600 µL of ice-cold HBSS, flash-frozen in liquid nitrogen, and stored at -80 °C until analysis.

Relative quantification in LC-MS/MS intracellular accumulation assays

LC-MS/MS intracellular accumulation assays were performed in collaboration with the Pharmacology Core at the University of Texas Southwestern Medical Center (UTSW). LC-MS/MS assays were performed as described in [8] with the following modification – instead of calculating a quantitative assessment of the absolute amount of compound in each sample, a relative assessment was performed. This method allowed us to quantify the change – if any – in the relative amount of compound present in the samples when TQR was added. An increase in the relative amount of compound indicates enhanced intracellular retention that compound. This quantification method can be described using the following equations:

(0.1) $$ratio\ analyte\ /\ internal\ standard\ (IS)\ = \frac{analyte\ peak\ area\ (counts)}{IS\ peak\ area\ (counts)}$$

(0.2) $$normalized\ ratio\ = \frac{ratio\ of\ analyte\ /\ IS}{sample\ content\ (mg\ /\ ml)}$$

(0.3) $$mean\ ratio = \frac{\sum_{i=1}^{n} ratio_i}{n\ samples}$$

where "Analyte" refers to the experimental compound tested. The "Internal Standard" (IS) is a known substance added in a constant amount to each sample. The "Peak Area", expressed as "counts", describes the number of MS/MS spectra from the experimental compound and serves as a measure of its relative abundance. For each sample, the relative abundance of experimental compound is expressed as a ratio of the Analyte abundance divided by the Internal Standard abundance equation (0.1). To account for any differences in the amount of cell lysate between samples, the ratio of each sample is normalized to its respective cell lysate content expressed in mg / mL, as shown in equation (0.2). Lastly, as shown in equation (0.3), we average the "Normalized Ratio" of the samples, performed in triplicate, to produce the final values shown in Supplemental Table 2. These values allow a comparison of the relative abundance of compound between the "- TQR" and "+ TQR" samples, and to test for statistically significant differences.

Sample preparation and analysis with LC-MS/MS

LC-MS/MS quantification was performed as follows. Cell lysate was aliquoted into Eppendorf tubes. In contrast to [8], blank cell lysates were not spiked with varying concentrations of each compound to create a standard curve, since compound amounts were

normalized to abundance of the internal standard. Instead, after the initial aliquot step, MeOH containing 50 ng/mL N-Benzylbenzamide was added to each sample. Samples were vortexed briefly, incubated at 27 °C for 10 minutes, and spun at 13,200 RPM for 5 minutes. The supernatant was transferred to a new Eppendorf tube and spun once more at 13,200 RPM for 5 minutes. The supernatant was then transferred to an HPCL vial, and subsequently analyzed using LC-MS/MS using a Sciex 4000QTRAP mass spectrometer coupled to a Shimadzu Prominence LC.

Chromatography conditions were as follows: Buffer A contained water + 0.1% formic acid, and Buffer B contained methanol + 0.1% formic acid. The column flow rate was 1.5 ml/min using an Agilent C18 XDB, 5 micron packing 50 × 4.6 mm column. After the addition of the organic solvent, the remaining cell lysate was resuspended in 0.1 M NaOH, boiled for 5 min, and mixed with 1:50 B:A reagent (Thermofisher BCA Kit) to determine the cell lysate concentration in each sample. A BSA standard curve was then prepared in water and mixed using the same ratio. The samples were incubated 30 min at 37 °C and read at 562 nm. The ratio of Analyte to Internal Standard was normalized to the lysate content for each individual sample. The data for each trial are shown in Supplemental Table 2. Statistical significance was determined using a Student's T Test in GraphPad Prism.

Daunorubicin accumulation assays

These assays are based upon those reported in [8]. DU145-TXR cells were seeded in 96 well plates in complete RPMI medium at 15,000 cells per well. Cells were allowed to grow for 48 hours in a humidified incubator at 37 °C and 5% CO_2. After 48 hours, media was replaced with fresh complete RPMI medium. Cells were treated with 10 µM of experimental compound with or without 10 µM daunorubicin (DAU). After a 2-hour incubation at 37 °C and 5% CO_2 in a humidified incubator, media was removed with a vacuum aspirator, and cells were washed twice with ice-cold phosphate buffered saline (PBS) solution. Cells were lysed in PBS containing 0.5% SDS and 0.5% Triton X-100 and shaken on an Orbital Shaker for 10 min at 500 rpm. DAU fluorescence was read using the Cytation5 plate reader at excitation/emission 488 nm / 575 nm. Data are the mean ± one standard deviation from three independent experiments, n = 3 samples per experiment, n = 9 total. Statistical significance was determined with a Student's T test in GraphPad prism. None of the experimental compounds exhibited significant background fluorescence at the tested excitation and emission range.

$$\Delta\, DAU\ Fluorescence = \frac{Fluorescence\ of\ (Compound + DAU)\ treated\ cells}{Fluorescence\ of\ DAU\ treated\ cells}$$

RESULTS

Computational screens identify putative P-gp inhibitors for testing *in vitro*

We used molecular docking to computationally screen thousands of molecules for their potential binding affinity to P-gp. Docking screens were specifically designed to select for molecules that preferentially bind to the nucleotide binding domains, and that do not strongly interact with the drug binding domains. In previous work by us [6, 7], molecules were docked to a model of human P-gp that was in an open-to-the-outside conformation [6, 30], where the nucleotide binding domains are closely engaged and the drug binding domains are widely open to the extracellular side of the membrane. Molecules that were predicted to preferentially bind the transmembrane drug binding domains were not taken into consideration for future studies.

A limitation of this earlier approach was that the open-to-the-outside structure represents the end of the transport cycle, where pump substrates likely are released to the cell exterior. It therefore may not represent the best conformation for screening for P-gp inhibitors that are not transport substrates themselves. To identify inhibitors that are not P-gp transport substrates, it was deemed important to screen for affinity of binding to the DBD conformation at the beginning of a transport cycle, where the DBDs are open to the cytoplasm and ready to capture substrates. However, suitable open-to-the-inside structures were (and are still) not available for human P-gp. To overcome this limitation, we used targeted Molecular Dynamics (tMD) simulations to guide a model of human P-gp through conformational changes that are likely representative of a drug transport cycle (see Methods) [17]. These MD trajectories were then used to generate a number of open-to-the-inside and open-to-the-outside conformations for molecular docking experiments (Figure 1). Docking search boxes were designed to sample the small molecule binding of five nucleotide binding and three drug binding domain conformations of P-gp (Supplemental Figure 1). The goal was to identify small drug like compounds that prefer the NBDs over the DBDs.

Autodock Vina [24] was used to screen molecules from the ZINC12 clean, drug-like (CDL) library against dynamic P-gp structures from tMD simulations. Our previous computational screen targeted only one conformation of P-gp; here we expand the screening to 14 different structures and locations. This increase in the number of times each molecule is iteratively screened necessitated to find a more efficient way to screen the drug libraries in an acceptable time frame. Tanimoto sets are a useful tool for reducing a molecule dataset to a more tractable size [31]. The Tanimoto algorithm determines the similarity between molecules in a dataset and uses that metric to select molecules that are representative of the chemical diversity in that dataset. In the experiments described here, Tanimoto sets were used to trim the original CDL library from ~13 million compounds to 123,000 - 158,000 molecules (see Methods). If a molecule from the Tanimoto set performed well in docking screens, similar molecules were collected from the CDL dataset and screened against the same P-gp targets.

Using this iterative approach, 95% of the chemical diversity within the CDL library was efficiently screened for estimated affinity to the DBDs and the NBDs of P-gp. Molecules with low estimated affinities at the DBDs and *high* estimated affinities at the *NBDs* were retained during each iterative round of molecular docking, as described in [6] (Supplemental Figure 2). After the final docking screen, the top 100 molecules against each P-gp target structure were subjected to quantitative structure-activity relationship (QSAR) predictions using the Online chemical database (OCHEM) [26]. The QSAR data, select predicted chemical properties, and estimated binding affinities were used to select 67 compounds for testing with cell-based assays. The experimental compounds were numbered 58 to 124 in order of arrival to the laboratory [25].

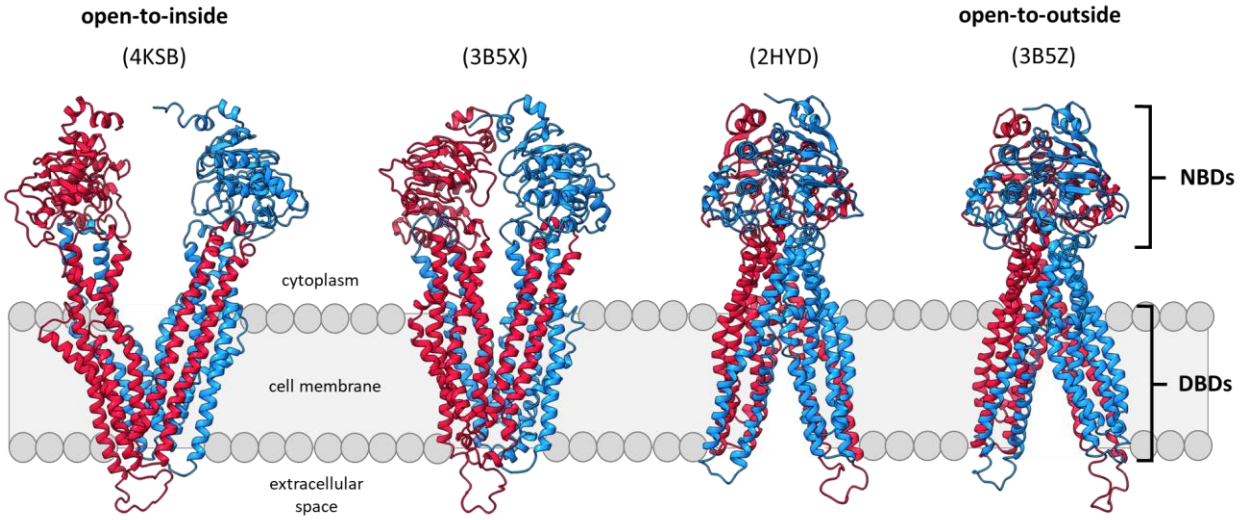

Figure 1. Structures of human P-gp used for molecular docking screens. P-gp adopts several dynamic conformations during the substrate transport cycle. The cytoplasmic NBDs bind and hydrolyze ATP, while the membrane-embedded DBDs capture and transport substrates. P-gp switches from 'open-to-inside/cytoplasm' to 'open-to-outside/extracellular space' conformation during transport, thereby alternating substrate access from the cytoplasm to the extracellular space. Search boxes for docking experiments were designed to sample the NBDs or DBDs of human P-gp in each of these conformations. The source PDB ID for each target conformation shown is in parentheses above each conformation [32-34].

Potential P-gp inhibitors reverse MDR in P-gp-overexpressing prostate cancer cells

The computationally identified compounds were screened for the ability to re-sensitize P-gp overexpressing DU145-TXR cancer cells to paclitaxel (PTX), a chemotherapeutic drug and transport substrate of P-gp [28]. DU145-TXR cells greatly overexpress P-gp relative to the DU145 parental cells and exhibit a 34-fold increase in the IC_{50} of PTX relative to that of DU145 cells [28]. In the described experiments, re-sensitization was defined as a 30% or greater decrease in cell

viability between cells treated with PTX alone, or with a combination of PTX and the experimental compound. DU145-TXR cells were exposed to compounds 58 to 124 at 15 µM, with or without 500 nM PTX, for 48 hours. Cell viability was then assessed with MTT viability assays as previously described [8]. Tariquidar and verapamil were included as positive controls for P-gp inhibition, and the BCRP inhibitor Ko143 was included as a negative control for P-gp inhibition [35]. Treatment with 11 compounds (61, 68, 70, 78, 96, 97, 101, 103, 111, 122, 124) re-sensitized DU145-TXR cells to PTX (Figure 2A, Supplemental Table 6). The remaining compounds were eliminated from further consideration as potential P-gp inhibitors.

The 11 compounds that re-sensitized DU145-TXR cells to PTX (Figure 2A) were then tested for their ability to sensitize the parental line DU145 cells to PTX [28]. Our hypothesis was that since DU145 cells do not overexpress P-gp, a compound that enhances PTX toxicity in DU145 cells is unlikely to act solely by inhibiting P-gp transport, but may have a different cellular target. In these experiments, DU145 cells were exposed to the experimental compounds at 15 µM in the presence or absence of PTX and cell viability was assessed using MTT assays. Nine of the 11 compounds tested (compounds 70, 78, 96, 97, 101, 103, 111, 122, and 124) were observed to insignificantly sensitize DU145 cells to PTX (Figure 2B) as compared to exposing the cells to PTX alone, see dotted line and PTX toxicity in the absence of compounds. Except for compound 68, the top hits were not observed to exhibit significant intrinsic toxicity against DU145 cells. Verapamil is known to cause significant off-target effects [10], so its effect on non-P-gp overexpressing DU145 was not really surprising.

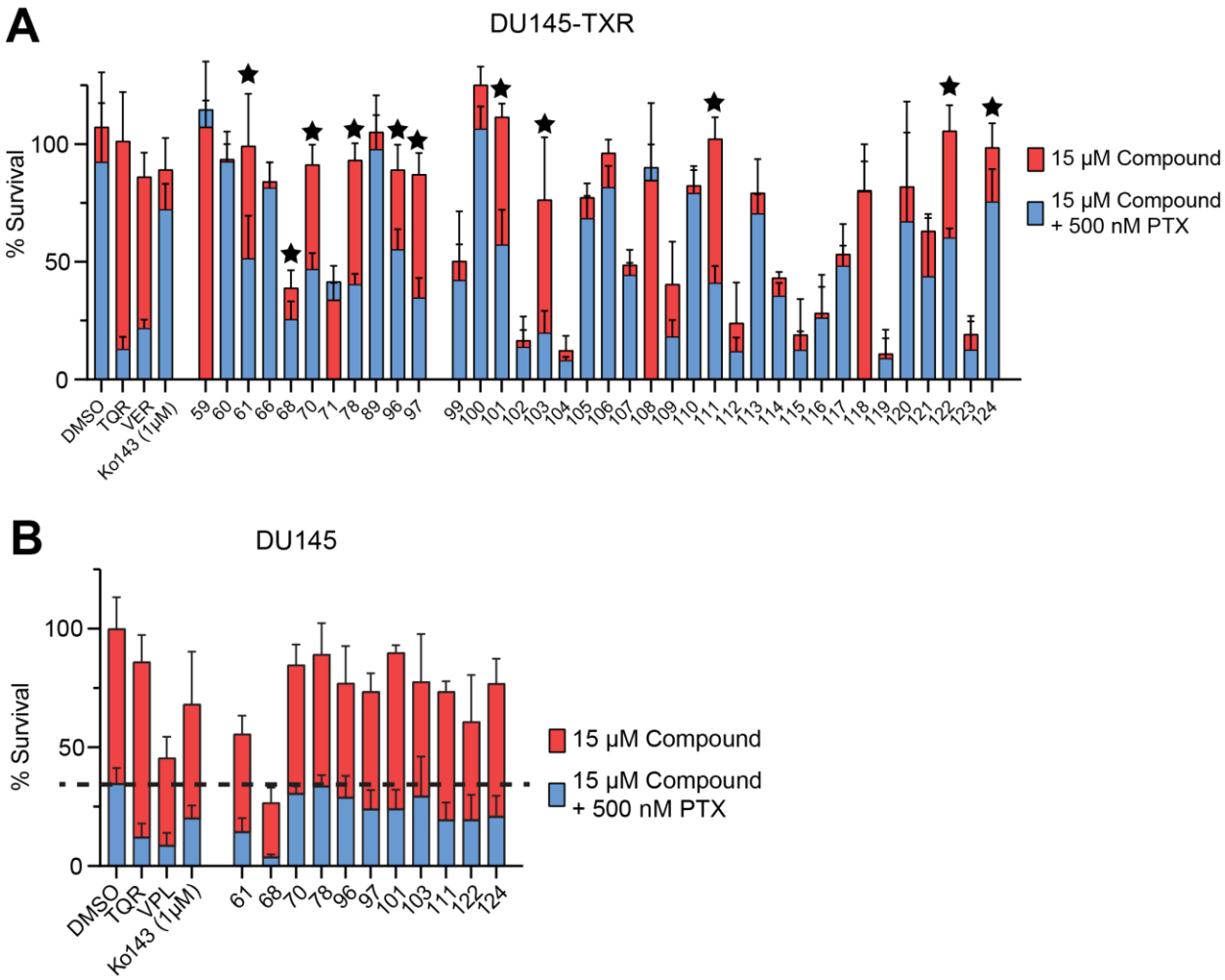

Figure 2: Potential P-gp inhibitors reverse MDR in P-gp overexpressing DU145-TXR cancer cells. 67 compounds were chosen from computational screens for testing *in vitro*. **A)** DU145-TXR cells were exposed to 15 μM experimental compound with or without 500 nM of the P-gp substrate and chemotherapeutic paclitaxel (PTX). Tariquidar (TQR) and verapamil (VPL) at 15 μM were used as positive controls for P-gp inhibition, while Ko143 at 1 μM and DMSO vehicle control were used as negative controls for P-gp inhibition. Percent (%) survival is calculated as the percent survival relative to that of the vehicle control (DMSO-treated) cells (see Methods). Starred compounds are considered 'top hits'. **B)** Top compounds were tested for inherent toxicity with the non-P-gp overexpressing DU145 parental line. Cells were exposed to 15 μM compound with or without 500 nM PTX for 48 hours, after which cell viability was assessed using the MTT viability assay. Data represent the mean ± one standard deviation from the mean (n = 8, two independent trials).

Potential P-gp inhibitors are not specific to one cancer cell line

To test if the potential P-gp inhibitors were specific to DU145-TXR cancer cells, the top compounds (70, 78, 96, 97, 101, 103, 111, 122 and 124) were tested with second set of paired

cancer cell lines – the P-gp overexpressing, doxorubicin resistant A2780-ADR ovarian cancer cell line, and the parental, non-P-gp overexpressing A2780 line [8, 36, 37]. Doxorubicin is both a chemotherapeutic and a P-gp transport substrate. Since it is possible that the resistance of the A2780-ADR cell line to Doxorubicin involves mechanisms other than P-gp overexpression, assays used PTX to test for the potential to reverse MDR. Tariquidar and verapamil were used as positive controls for P-gp inhibition, with the BCRP inhibitor, Ko143, as a negative control. Compound 59 was used as an additional negative control because it did not reverse MDR in DU145-TXR cells (Figure 2A). Of the nine compounds tested against DU145-TXR, each compound (70, 78, 96, 97, 101, 103, 111, 122, and 124) also reversed MDR in A2780-ADR cells (Figure 3A), but did not greatly increase the toxicity of PTX against the parental A2780 cells (Figure 3B, dashed line represents the effect of 500 nM PTX alone). These nine compounds (70, 78, 96, 97, 101, 103, 111, 122, and 124) were therefore considered to be good candidates for further toxicity testing and for evaluation as potential P-gp pump substrates.

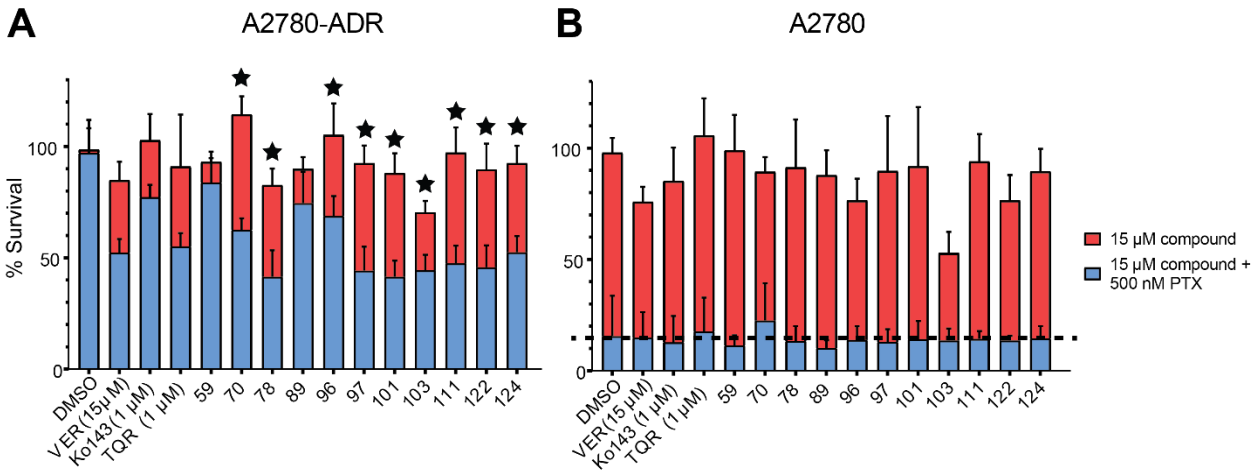

Figure 3: Putative P-gp inhibitors reverse MDR in P-gp-overexpressing A2780-ADR cancer cells.

The top 10 compounds from screens with DU145 and DU145-TXR were tested at 15 µM concentration against **A)** the chemotherapy-resistant, P-gp overexpressing A2780-ADR line and **B)** the chemotherapy-sensitive, non-P-gp overexpressing parental A2780 line. Cells were exposed to compounds with or without 500 nM Paclitaxel (PTX) for 48 hours. The vehicle (DMSO) control represents PTX toxicity in the absence of compound (dotted line). Cell viability was assessed using the MTT viability assay. Data represent the mean ± one standard deviation from the mean, n = 8, from at least two trials. Compounds 59 and 89 were used as internal negative controls for compounds that did not reverse MDR in DU145-TXR cells (Figure 2A). Starred compounds in panel **A)** were considered to be the top hits.

Experimental compounds are not substantially toxic to non-cancerous human cells

If a P-gp inhibitor is intrinsically toxic to non-cancerous cells, it is more likely to be participating in undesirable off-target interactions. The top compounds from the screens shown

above were screened for inherent toxicity using the non-cancerous HFL1 (human lung fibroblast) cell line [38]. HFL1 cells were incubated with 15 µM compound for 48 hours, after which cell viability was assessed using MTT cell viability assays. A 20% reduction in cell viability (compared to DMSO-treated cells) was considered the maximum acceptable toxicity (see dotted line). The chemotherapeutic daunorubicin was included as a positive control for toxicity. Nine compounds (70, 78, 96, 97, 101, 103, 111, 122 and 124) were deemed by us as either 'non-toxic' or 'within acceptable limits' of toxicity (Figure 4).

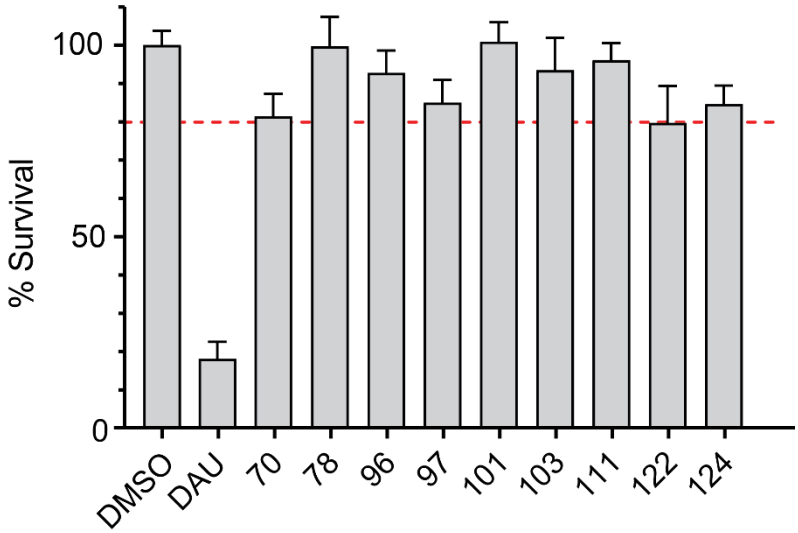

Figure 4. Evaluating the inherent toxicity of potential P-gp inhibitors. The top compounds from previous screens were tested against the non-cancerous HFL1 cell line. HFL1 cells were exposed to 15 µM of experimental compound. Daunorubicin (DAU) was used as a positive control for inherent toxicity. Cells were exposed to the experimental treatments for 48 hours, after which cell viability was assessed using MTT viability assays. Data represent the mean ± one standard deviation from the mean (n = 8) from at least two independent experiments. The dashed line marks 80% viability of DMSO-treated cells. All of the experimental compounds were deemed to have tolerable toxicity.

Potential P-gp inhibitors are not transport substrates of P-gp

We aimed to identify P-gp inhibitors that are not transport substrates of the pump itself. To that end, our subtractive docking methods selected molecules that were predicted to favor the NDBs over the DBDs. To test these predictions *in vitro*, liquid chromatography with tandem mass spectrometry (LC-MS/MS) was used to assess the intracellular accumulation of experimental compounds as described in [8]. The P-gp overexpressing DU145-TXR cells were exposed to 5 µM compound with or without 500 nM tariquidar for 2.5 hours. At 500 nM concentration, tariquidar should strongly inhibit P-gp while not being transported itself [16]. The relative intracellular accumulation of each experimental compound was then assessed using LC-MS/MS. If the compound is a P-gp transport substrates, it should accumulate intracellularly in

the presence of tariquidar (P-gp inhibited), while the intracellular concentration should be lower in the absence of tariquidar (P-gp active). The P-gp substrate and chemotherapeutic daunorubicin (DAU) was used as a positive control for P-gp-mediated transport. Six of the compounds that reversed MDR in DU145-TXR and A2780-ADR cells (70, 78, 96, 97, 101, and 111) were deemed unlikely to be transport substrates of P-gp (Table 1 and Supplemental Table 2). Three compounds (103, 122 and 124) were found to be potential P-gp transport substrates.

Table 1. **Intracellular accumulation of compounds measured by LC-MS/MS.** The intracellular accumulation of each experimental compound was assessed in P-gp overexpressing DU145-TXR cells using LC-MS/MS with or without 500 nM Tariquidar. Significance was determined using a Student's T test of the mean; P > 0.05 = not significant (N.S.), P < 0.05 = *, P < 0.01 = **, P < 0.001 = ***, P < 0.0001 = ****. A statistically significant difference indicates that the experimental compound accumulated intracellularly in the presence of tariquidar, and is therefore likely to be transport substrate of P-gp. Samples were prepared in triplicate in two trials (n = 6). Compounds 78 and 103 were tested with three trials (n = 9). The P-gp substrate and chemotherapeutic daunorubicin (DAU) was included as a positive control for transport by P-gp.

	Trial 1			Trial 2			Trial 3		
	- TQR	+ TQR	P	- TQR	+ TQR	P	- TQR	+ TQR	P
DAU	0.014 ± 0.001	0.216 ± 0.002	$< 1x10^{-6}$ (****)	0.017 ± 0.001	0.232 ± 0.016	$2x10^{-5}$ (****)			
70	0.93 ± 0.15	0.93 ± 0.07	>1 (N.S.)	0.56 ± 0.11	0.55 ± 0.15	0.9 (N.S.)			
78	0.001 ± 0.000	0.001 ± 0.000	--	0.001 ± 0.000	0.001 ± 0.000	--			
96	0.087 ± 0.009	0.092 ± 0.036	0.8 (N.S.)	0.121 ± 0.005	0.163 ± 0.032	0.09 (N.S.)			
97	0.07 ± 0.02	0.08 ± 0.03	0.7 (N.S.)	0.10 ± 0.02	0.10 ± 0.02	> 1 (N.S.)			
101	11.86 ± 1.16	12.03 ± 2.45	0.9 (N.S.)	21.17 ± 3.59	22.88 ± 2.92	0.6 (N.S.)			
103	5.13 ± 0.6	5.61 ± 1.34	0.6 (N.S.)	2.63 ± 0.52	3.75 ± 0.34	0.04 (*)	3.21 ± 0.23	3.73 ± 0.15	0.03 (*)
111	0.012 ± 0.002	0.013 ± 0.004	0.7 (N.S.)	0.011 ± 0.002	0.013 ± 0.001	0.2 (N.S.)			
122	0.049 ± 0.005	0.146 ± 0.018	0.0008 (***)	0.058 ± 0.018	0.209 ± 0.014	0.0003 (***)			
124	0.006 ± 0.001	0.061 ± 0.011	0.001 (**)	0.007 ± 0.002	0.055 ± 0.009	0.0008 (***)			

Experimental compounds inhibit the transport of a P-gp substrate

To ensure that the top candidates from our previous studies were indeed targeting and inhibiting P-gp activity, we tested these compounds for their ability to enhance intracellular accumulation of the P-gp substrate, daunorubicin (DAU). These assays used the P-gp highly overexpressing DU145-TXR cell line. In this assay, the intrinsic fluorescence of DAU was used to quantify its relative concentration in the cell. An increase in fluorescence correlates with an increase in the intracellular accumulation of DAU. Compounds 70, 78, 96, 97, 101, 103, 111

were assessed for the ability to increase the intracellular retention of DAU. Compound 59 was included as a negative control for P-gp inhibition, tariquidar and verapamil were included as positive controls for P-gp inhibition. Cells were treated with 10 µM of experimental compound with or without 10 µM DAU. After a 2-hour incubation, cells were washed and lysed, and the total fluorescence of DAU in each well was quantified. Treatment with compounds 70, 96, 97, and 101, and 103 significantly increased the DAU fluorescence in DU145-TXR cells, indicating an increase in the intracellular retention of DAU (Figure 5 and Supplemental Table 3). As expected, treatment with compound 59 did not significantly increase fluorescence of DAU. The results of these assays suggest that compounds 70, 96, 97, 101, and 103 significantly inhibited transport of DAU by P-gp. Compounds 78 and 111 did not cause an increase in intracellular DAU retention. Together with LC-MS/MS data, our results suggest that compounds 70, 96, 97, and 101 are not P-gp substrates, and therefore are more likely to bind at the cytoplasmic NBDs, which were targeted our docking studies.

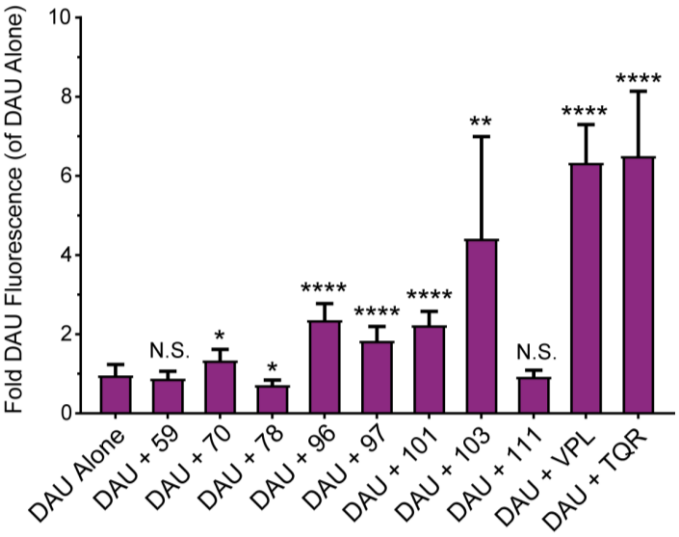

Figure 5. Change in Fluorescence of DAU in the Presence of Experimental Compounds. Fold change in fluorescence of the P-gp substrate Daunorubicin (DAU) in the presence or absence of experimental compounds or known P-gp modulators. Cells were treated with 10 µM compound in the presence or absence of 10 µM DAU. After washing and lysing the cells, the intracellular DAU fluorescence was measured and expressed as a fold change relative to the fluorescence of DU145-TXR cells treated with DAU alone. The P-gp inhibitors, VPL and TQR, were included as positive controls for P-gp inhibition, and compound 59 was included as a negative control for P-gp inhibition. N = 9, with three samples per trial, three trials. Significance was determined using a Student's T test of the mean; $P > 0.05$ = N.S., $P < 0.05$ = *, $P < 0.01$ = **, $P < 0.001$ = ***, $P < 0.0001$ = ****.

DISCUSSION

Multidrug resistance is a major obstacle to the treatment of human cancer. As prominent causes for multidrug resistance, ABC transporters like P-gp are clinically-relevant targets [1].

However, decades of studies have shown that these proteins are also notoriously difficult to target in drug discovery. The dynamic nature of ABC transporters lies at the heart of the difficulty in targeting these pumps. ABC transporters move their substrates by undergoing substantial conformational changes that significantly rearrange the nucleotide binding domains (NBDs) and drug binding domains (DBDs) during transport (Figure 1). Many of these conformational changes – particularly how P-gp transitions from open-to-inside to open-to-outside conformations – remain poorly understood because it is not currently possible to observe transport directly. Because of these structural rearrangements, target sites for small molecule inhibitors change substantially throughout the transport cycle of P-gp, making it increasingly hard to design respective molecules.

We previously provided evidence that P-gp can accommodate and pump molecules as bulky as the amyloid β peptides [5]. Additional computational analyses of drug transport suggested that substrates may have multiple pathways through the DBDs [17]. Binding sites for small molecule inhibitors in the DBDs are abundant, but P-gp inhibitors that target the DBDs tend to also be transport substrates (Supplemental Table 1) and have performed poorly in clinical trials. Even though efforts to target P-gp have yielded three generations of clinically unsuccessful inhibitors, the pump remains an important target in the fight against multidrug resistance [1].

In earlier work, we demonstrated that the pump's cytoplasmic NBDs are viable targets for drug discovery [6-9, 39]. These early screens targeted the NBDs and used subtractive molecular docking to only one conformation of the pump, where the NBDs are closely engaged and the DBD are open to the outside (6) identified four compounds that reversed MDR in cancer, with an impressive ~ 7% hit rate [6, 7]. Subsequent work by us showed that optimization of one of the compounds, SMU 29, successfully yielded more novel P-gp inhibitors that reversed MDR in cancer [9, 39].

Here we built upon this earlier work to create an enhanced screening pipeline, with the goal of identifying more P-gp inhibitors that target the NBDs and reverse MDR in human cancers. Novel counter-selective docking techniques were used to virtually screen millions of compounds against dynamic structures of P-gp, with the goal of selecting molecules that target the pump's NBDs. Of the 67 compounds identified through docking, nine reversed MDR in human cancer cell lines, a 14% hit rate for compounds that reverse MDR. These compounds were shown to be non-toxic to non-cancerous cells and were effective in the 15 µM range. They are therefore deemed to be good candidates for lead optimization (Figure 6).

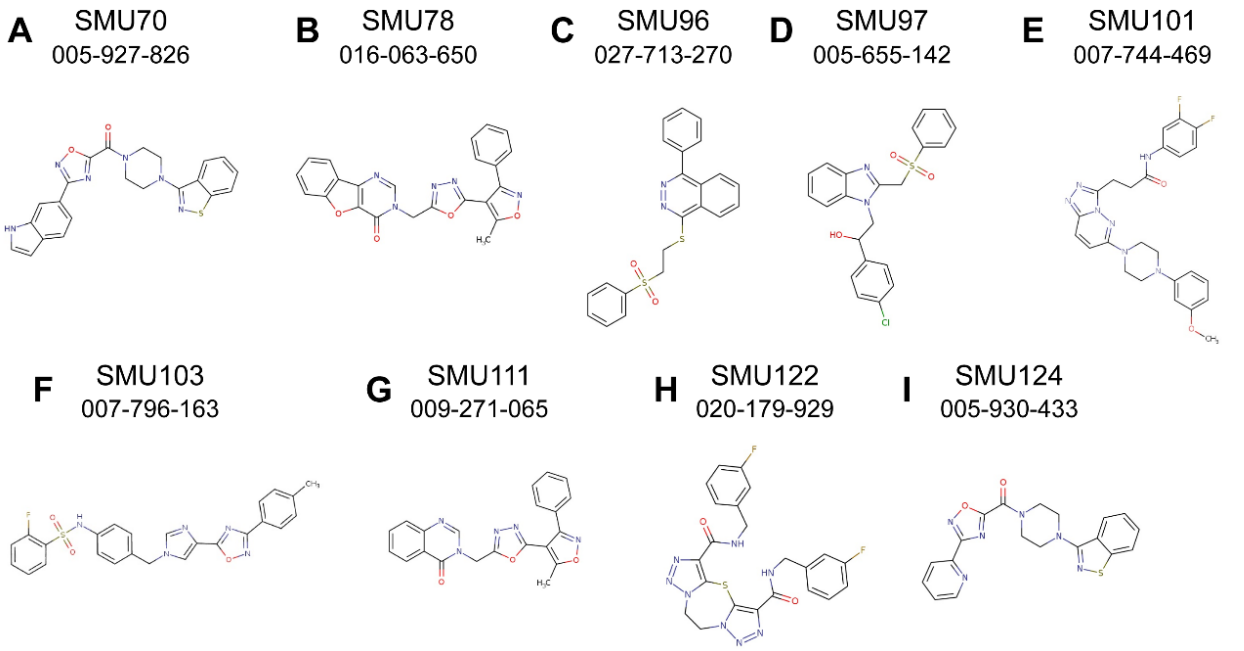

Figure 6. Structures of novel P-gp inhibitors identified by virtual-assisted drug discovery. Chemical structures of the nine best P-gp inhibitors identified in this study (panels A through I) with our laboratory name (SMU-) above, and the MolPort identification number below. The ZINC identification number, IUPAC International Chemical Identifier (InChI) key, and the Simplified Molecular Input Line Entry System (SMILES) code for each molecule are listed in Supplemental Table 5.

The success rate of 14% with an effective dose of 15 µM represents an enhancement of traditional computational screening methods by a significant factor. For identification of lead compounds that are effective at < 100 µM concentrations, the median hit rate of virtual-assisted efforts is approximately 13% (34). 103 studies reported hit rates greater than 25%; however, 75% of these studies tested fewer than 20 compounds and used a sub-100 µM dose as their minimal dose cutoff (21). These trends of small sample size and very high dose concentration cut-offs have been observed in other virtual-assisted studies (35-37).

Many virtual-assisted studies benefited from high-resolution the target proteins, frequently including co-crystallized inhibitors. When the docking studies presented here were performed, such suitable structures were not available and even to date, no high-resolution structural data exist for human P-gp during its complete conformational transport cycle. As an additional factor, the available structures of P-gp homologues were limited both in resolution and in conformational diversity. To overcome this limitation and produce suitable structures for molecular docking, we built a homology model of human P-gp and used targeted MD to generate structural 'snapshots' of the transporter throughout a putative catalytic transport cycle [17, 30]. The 7% hit rate of our proof-of-concept drug discovery studies using this model [6, 7], and the two-fold increase (14%) in hit rate for the work presented here, reinforce and validate

the use of our P-gp model to virtually screen small molecules, and the use of counter-selective docking techniques to target the NBDs.

By targeting the NBDs, we have identified several P-gp inhibitors that are unlikely to be transport substrates of the pump itself (Figure 6). This was the goal of the counter-selective docking techniques, where the ratio of estimated affinities to the DBDs and NBDs was used to select molecules that potentially preferred the NBDs. The predicted binding affinity ratios of DBD-to-NBD for the top compounds identified in this work are shown in Supplemental Table 4. The hit rate for compounds that reverse MDR without being P-gp transport substrates is 7% (70, 78, 96, 97, 101, 111). However, the remaining top hits (103, 122, and 124) may still be considered successful even though they tested likely to be P-gp transport substrates, because lead-optimization could potentially produce variants that are less likely to be substrates. Thus, we feel that the nine compounds identified in this work could form the basis for a 4th generation of P-gp inhibitors (9-12).

Identifying P-gp inhibitors that are not transport substrates remains inherently challenging. To that end, computational tools such as the SWISS-ADME server attempt to use a molecule's unique chemical and structural characteristics to predict whether it is likely to be a P-gp transport substrate [40]. Our LC-MS/MS assays allowed us to retroactively test the validity of predictions from SWISS-ADME. Of 13 compounds assayed in total using LC-MS/MS (not all data shown), only four were correctly predicted to be P-gp transport substrates. This discrepancy underscores the inherent difficulty of computationally predicting transport substrates of this dynamic ABC transporter. We have also included the SWISS-ADME analyses of molecular weight, topological polar surface area, Log $P_{oct/wat}$ (hydrophobicity), and Log S (water solubility) for our top hits from this work, as well as for several compounds that did not reverse MDR, in hopes that these data can be used to guide selection of future P-gp inhibitors for screening. Alternative identifiers for the molecules identified in this study are shown in Supplemental Table 5.

Table 2. **Computational analysis of compounds and comparison to *in vitro* data**. The top performing compounds from *in vitro* assays against DU145-TXR were subjected to post-hoc analysis with SWISS-ADME [40]. Compounds 59 and 89 were included as examples of compounds with significantly different properties that did not reverse MDR; 59 and 89 were used as internal negative controls for P-gp inhibition with the A2780-ADR and A2780 cell lines. The predicted aqueous solubility was compared to that observed in the laboratory. The predicted classification as a P-gp substrate was compared to the LC-MS/MS intracellular accumulation data, if available. ND = no data. $LogP_{oct/wat}$ and LogS are reported as the Consensus values calculated with SWISS-ADME. Top Hits are compounds that 1) reverse MDR, 2) do not increase PTX toxicity in chemo-sensitive cancer cells, 3) are non-toxic to noncancerous cells, and 4) are not P-gp substrates.

#	MW (g/mol)	TPSA (Å^2)	Log $P_{oct/wat}$	LogS	Correct Water Solubility Prediction?	Predicted to be P-gp Substrate	Correct P-gp Substrate Prediction?	MolPort #	Top Hit
59	323	189	-0.59	Soluble	Yes	Yes	ND	002-662-098	No
60	522	146	3.88	Poorly	No	Yes	No	000-779-897	No
61	480	164	0.3	Soluble	No	Yes	Yes	001-984-582	No
66	411	121	1.74	Soluble	Yes	Yes	No	005-923-195	No
70	430	120	3.23	Poorly	Yes	Yes	No	005-927-826	**Yes**
71	455	104	3.74	Poorly	Yes	Yes	No	005-926-380	No
78	425	113	3.28	Moderate	Yes	Yes	No	016-063-650	**Yes**
79	342	64	3.62	Moderate	Yes	Yes	ND	005-914-703	No
89	354	167	0.42	Soluble	Yes	Yes	ND	005-754-407	No
96	407	94	4.49	Poorly	No	No	Yes	027-713-270	**Yes**
97	427	81	3.8	Moderate	Yes	No	Yes	005-655-142	**Yes**
101	494	88	3.28	Moderate	Yes	Yes	No	007-744-469	**Yes**
103	490	111	4.11	Poorly	No	No	No	007-796-163	No
111	385	100	2.97	Moderate	Yes	Yes	No	009-271-065	**Yes**
122	496	145	2.65	Moderate	Yes	Yes	Yes	020-179-929	No
124	392	116	2.38	Moderate	Yes	No	No	005-930-433	No

The ABC transporter superfamily contains many proteins that undergo similar conformational dynamics to P-gp [1, 2]. One of the most clinically-relevant is breast cancer resistance protein (BCRP, *ABCG2*), which confers MDR to several types of human cancers [41-43]. Similar to P-gp, BCRP also consists of cytoplasmic NBDs and membrane-embedded DBDs, and previous drug discovery efforts have focused on the DBDs [44]. DBD-targeted BCRP inhibitors have exhibited problems with poor solubility, principally because molecules that bind to the DBDs tend to be hydrophobic [44]. The NDBs, however, have not been thoroughly explored in drug discovery. Based upon the success of our method, we suggest that the NBDs of BCRP are good candidates for virtual-assisted drug discovery. High-resolution structures of BCRP are increasingly available in several conformations, which will enhance counter-selective docking screens similar to those used here [45-48].

Following recent advances in cryo-EM, high-resolution structures of ABC transporters are increasingly available for use in virtual screening efforts [4, 16]. The methodology presented here, particularly the use of counter-selective docking methods, could be applied to drug screens targeting many members of the ABC transporter family – and perhaps other families of dynamic transporters. In addition to conferring MDR to cancers, ABC transporters like Msba from *E. coli* also perform essential functions in pathogenic bacteria. Targeting bacterial ABC transporters with the counter-selective docking methods presented here could aid in the fight against drug resistant bacterial infections [49].

DECLARATIONS

Acknowledgements

We acknowledge the help of Ms. Jesiska Lowe in preparing the accumulation assays.

Author's contributions

Lauren A. McCormick – conceptualization, visualization, methodology, analysis, writing – original draft, review, editing

James W. McCormick – conceptualization, visualization, methodology, analysis, writing – original draft, review, editing

Chanyang Park – investigation, visualization, editing

John G. Wise – conceptualization, supervision, funding acquisition, review and editing

Pia D. Vogel – conceptualization, supervision, funding acquisition, review and editing

Availability of data and materials

All data are available upon reasonable request.

Financial support and sponsorship

This work is supported by NIH NIGMS [R15GM09477102] to JGW/PDV, SMU University Research Council, SMU Engaged Learning program, the SMU Center for Drug Discovery, Design and Delivery, the Communities Foundation of Texas, and private gifts from Ms. Jane Henderson, New York, New York. We thank Robert Harrod, Southern Methodist University, Dallas, TX, for the gift of the HFL1 cells, as well as Evan T Keller, University of Michigan, Ann Arbor MI, for the gift of the DU145 and DU145-TXR cells.

Conflicts of Interest

The authors declare no conflicts of interest.

Consent for Publication

The authors have given their consent to publish.

Copyright

© The Authors 2024

REFERENCES

(1) Juan-Carlos, P. M.; Perla-Lidia, P. P.; Stephanie-Talia, M. M.; Monica-Griselda, A. M.; Luz-Maria, T. E. ABC transporter superfamily. An updated overview, relevance in cancer multidrug resistance and perspectives with personalized medicine. *Mol Biol Rep* **2021**, *48* (2), 1883-1901. DOI: 10.1007/s11033-021-06155-w.

(2) Sharom, F. J. ABC multidrug transporters: structure, function and role in chemoresistance. *Pharmacogenomics* **2008**, *9* (1), 105-127. DOI: 10.2217/14622416.9.1.105.

(3) Bates, S. E.; Meadows, B.; Goldspiel, B. R.; Denicoff, A.; Le, T. B.; Tucker, E.; Steinberg, S. M.; Elwood, L. J. A pilot study of amiodarone with infusional doxorubicin or vinblastine in refractory breast cancer. *Cancer Chemother Pharmacol* **1995**, *35* (6), 457-463. DOI: 10.1007/BF00686829 From NLM Medline.

(4) Alam, A.; Kowal, J.; Broude, E.; Roninson, I.; Locher, K. P. Structural insight into substrate and inhibitor discrimination by human P-glycoprotein. *Science* **2019**, *363* (6428), 753-756. DOI: 10.1126/science.aav7102.

(5) McCormick, J. W.; Ammerman, L.; Chen, G.; Vogel, P. D.; Wise, J. G. Transport of Alzheimer's associated amyloid-beta catalyzed by P-glycoprotein. *PLoS One* **2021**, *16* (4), e0250371. DOI: 10.1371/journal.pone.0250371.

(6) Brewer, F. K.; Follit, C. A.; Vogel, P. D.; Wise, J. G. In silico screening for inhibitors of p-glycoprotein that target the nucleotide binding domains. *Mol Pharmacol* **2014**, *86* (6), 716-726. DOI: 10.1124/mol.114.095414.

(7) Follit, C. A.; Brewer, F. K.; Wise, J. G.; Vogel, P. D. In silico identified targeted inhibitors of P-glycoprotein overcome multidrug resistance in human cancer cells in culture. *Pharmacol Res Perspect* **2015**, *3* (5), e00170. DOI: 10.1002/prp2.170.

(8) Nanayakkara, A. K.; Follit, C. A.; Chen, G.; Williams, N. S.; Vogel, P. D.; Wise, J. G. Targeted inhibitors of P-glycoprotein increase chemotherapeutic-induced mortality of multidrug resistant tumor cells. *Sci Rep* **2018**, *8* (1), 967. DOI: 10.1038/s41598-018-19325-x.

(9) Wise, J. G.; Nanayakkara, A. K.; Aljowni, M.; Chen, G.; De Oliveira, M. C.; Ammerman, L.; Olengue, K.; Lippert, A. R.; Vogel, P. D. Optimizing Targeted Inhibitors of P-Glycoprotein Using Computational and Structure-Guided Approaches. *J Med Chem* **2019**, *62* (23), 10645-10663. DOI: 10.1021/acs.jmedchem.9b00966.

(10) Palmeira, A.; Sousa, E.; Vasconcelos, M. H.; Pinto, M. M. Three decades of P-gp inhibitors: skimming through several generations and scaffolds. *Curr Med Chem* **2012**, *19* (13), 1946-2025. DOI: 10.2174/092986712800167392.

(11) Robert, J.; Jarry, C. Multidrug resistance reversal agents. *J Med Chem* **2003**, *46* (23), 4805-4817. DOI: 10.1021/jm030183a.

(12) Litman, T.; Zeuthen, T.; Skovsgaard, T.; Stein, W. D. Competitive, non-competitive and cooperative interactions between substrates of P-glycoprotein as measured by its ATPase activity. *Biochim Biophys Acta* **1997**, *1361* (2), 169-176. DOI: 10.1016/s0925-4439(97)00027-6 From NLM Medline.

(13) Cripe, L. D.; Uno, H.; Paietta, E. M.; Litzow, M. R.; Ketterling, R. P.; Bennett, J. M.; Rowe, J. M.; Lazarus, H. M.; Luger, S.; Tallman, M. S. Zosuquidar, a novel modulator of P-glycoprotein, does not improve the outcome of older patients with newly diagnosed acute myeloid leukemia: a randomized, placebo-controlled trial of the Eastern Cooperative Oncology Group 3999. *Blood* **2010**, *116* (20), 4077-4085. DOI: 10.1182/blood-2010-04-277269.

(14) Kelly, R. J.; Draper, D.; Chen, C. C.; Robey, R. W.; Figg, W. D.; Piekarz, R. L.; Chen, X.; Gardner, E. R.; Balis, F. M.; Venkatesan, A. M.; et al. A pharmacodynamic study of docetaxel in combination with the P-glycoprotein antagonist tariquidar (XR9576) in patients with lung, ovarian, and cervical cancer. *Clin Cancer Res* **2011**, *17* (3), 569-580. DOI: 10.1158/1078-0432.CCR-10-1725.

(15) Bankstahl, J. P.; Bankstahl, M.; Romermann, K.; Wanek, T.; Stanek, J.; Windhorst, A. D.; Fedrowitz, M.; Erker, T.; Muller, M.; Loscher, W.; et al. Tariquidar and elacridar are dose-dependently transported by P-glycoprotein and Bcrp at the blood-brain barrier: a small-animal positron emission tomography and in vitro study. *Drug Metab Dispos* **2013**, *41* (4), 754-762. DOI: 10.1124/dmd.112.049148 From NLM Medline.
(16) Nosol, K.; Romane, K.; Irobalieva, R. N.; Alam, A.; Kowal, J.; Fujita, N.; Locher, K. P. Cryo-EM structures reveal distinct mechanisms of inhibition of the human multidrug transporter ABCB1. *Proc Natl Acad Sci U S A* **2020**, *117* (42), 26245-26253. DOI: 10.1073/pnas.2010264117.
(17) McCormick, J. W.; Vogel, P. D.; Wise, J. G. Multiple Drug Transport Pathways through Human P-Glycoprotein. *Biochemistry* **2015**, *54* (28), 4374-4390. DOI: 10.1021/acs.biochem.5b00018.
(18) Phillips, J. C.; Braun, R.; Wang, W.; Gumbart, J.; Tajkhorshid, E.; Villa, E.; Chipot, C.; Skeel, R. D.; Kale, L.; Schulten, K. Scalable molecular dynamics with NAMD. *J Comput Chem* **2005**, *26* (16), 1781-1802. DOI: 10.1002/jcc.20289.
(19) Morris, G. M.; Huey, R.; Lindstrom, W.; Sanner, M. F.; Belew, R. K.; Goodsell, D. S.; Olson, A. J. AutoDock4 and AutoDockTools4: Automated docking with selective receptor flexibility. *J Comput Chem* **2009**, *30* (16), 2785-2791. DOI: 10.1002/jcc.21256.
(20) *Molinspiration property calculation service*; https://www.molinspiration.com (accessed.
(21) Candee C. Chambers, G. D. H., Christopher J. Cramer, Donald G. Truhlar. Model for Aqueous Solvation Based on Class IV Atomic Charges and First Solvation Shell Effects. *J Phys Chem* **1996**, *100* (40), 16385-16398. DOI: https://doi.org/10.1021/jp9610776.
(22) Irwin, J. J.; Shoichet, B. K. ZINC--a free database of commercially available compounds for virtual screening. *J Chem Inf Model* **2005**, *45* (1), 177-182. DOI: 10.1021/ci049714+.
(23) O'Boyle, N. M.; Banck, M.; James, C. A.; Morley, C.; Vandermeersch, T.; Hutchison, G. R. Open Babel: An open chemical toolbox. *J Cheminform* **2011**, *3*, 33. DOI: 10.1186/1758-2946-3-33.
(24) Trott, O.; Olson, A. J. AutoDock Vina: improving the speed and accuracy of docking with a new scoring function, efficient optimization, and multithreading. *J Comput Chem* **2010**, *31* (2), 455-461. DOI: 10.1002/jcc.21334.
(25) Humphrey, W.; Dalke, A.; Schulten, K. VMD: visual molecular dynamics. *J Mol Graph* **1996**, *14* (1), 33-38, 27-38. DOI: 10.1016/0263-7855(96)00018-5.
(26) Sushko, I.; Novotarskyi, S.; Korner, R.; Pandey, A. K.; Rupp, M.; Teetz, W.; Brandmaier, S.; Abdelaziz, A.; Prokopenko, V. V.; Tanchuk, V. Y.; et al. Online chemical modeling environment (OCHEM): web platform for data storage, model development and publishing of chemical information. *J Comput Aided Mol Des* **2011**, *25* (6), 533-554. DOI: 10.1007/s10822-011-9440-2.
(27) Uzarski, J. S.; DiVito, M. D.; Wertheim, J. A.; Miller, W. M. Essential design considerations for the resazurin reduction assay to noninvasively quantify cell expansion within perfused extracellular matrix scaffolds. *Biomaterials* **2017**, *129*, 163-175. DOI: 10.1016/j.biomaterials.2017.02.015 From NLM Medline.
(28) Takeda, M.; Mizokami, A.; Mamiya, K.; Li, Y. Q.; Zhang, J.; Keller, E. T.; Namiki, M. The establishment of two paclitaxel-resistant prostate cancer cell lines and the mechanisms of paclitaxel resistance with two cell lines. *Prostate* **2007**, *67* (9), 955-967. DOI: 10.1002/pros.20581.
(29) van Meerloo, J.; Kaspers, G. J.; Cloos, J. Cell sensitivity assays: the MTT assay. *Methods Mol Biol* **2011**, *731*, 237-245. DOI: 10.1007/978-1-61779-080-5_20.
(30) Wise, J. G. Catalytic transitions in the human MDR1 P-glycoprotein drug binding sites. *Biochemistry* **2012**, *51* (25), 5125-5141. DOI: 10.1021/bi300299z.
(31) Irwin, J. J.; Sterling, T.; Mysinger, M. M.; Bolstad, E. S.; Coleman, R. G. ZINC: A Free Tool to Discover Chemistry for Biology. *J Chem Inf Model* **2012**, *52* (7), 1757-1768. DOI: 10.1021/ci3001277.
(32) Dawson, R. J.; Locher, K. P. Structure of a bacterial multidrug ABC transporter. *Nature* **2006**, *443* (7108), 180-185. DOI: 10.1038/nature05155.

(33) Ward, A.; Reyes, C. L.; Yu, J.; Roth, C. B.; Chang, G. Flexibility in the ABC transporter MsbA: Alternating access with a twist. *Proc Natl Acad Sci U S A* **2007**, *104* (48), 19005-19010. DOI: 10.1073/pnas.0709388104.
(34) Ward, A. B.; Szewczyk, P.; Grimard, V.; Lee, C. W.; Martinez, L.; Doshi, R.; Caya, A.; Villaluz, M.; Pardon, E.; Cregger, C.; et al. Structures of P-glycoprotein reveal its conformational flexibility and an epitope on the nucleotide-binding domain. *Proc Natl Acad Sci U S A* **2013**, *110* (33), 13386-13391. DOI: 10.1073/pnas.1309275110.
(35) Kannan, P.; Telu, S.; Shukla, S.; Ambudkar, S. V.; Pike, V. W.; Halldin, C.; Gottesman, M. M.; Innis, R. B.; Hall, M. D. The "specific" P-glycoprotein inhibitor Tariquidar is also a substrate and an inhibitor for breast cancer resistance protein (BCRP/ABCG2). *ACS Chem Neurosci* **2011**, *2* (2), 82-89. DOI: 10.1021/cn100078a.
(36) Hamilton, T. C.; Young, R. C.; Ozols, R. F. Experimental model systems of ovarian cancer: applications to the design and evaluation of new treatment approaches. *Semin Oncol* **1984**, *11* (3), 285-298. From NLM Medline.
(37) Rogan, A. M.; Hamilton, T. C.; Young, R. C.; Klecker, R. W., Jr.; Ozols, R. F. Reversal of adriamycin resistance by verapamil in human ovarian cancer. *Science* **1984**, *224* (4652), 994-996. DOI: 10.1126/science.6372095 From NLM Medline.
(38) Breul, S. D.; Bradley, K. H.; Hance, A. J.; Schafer, M. P.; Berg, R. A.; Crystal, R. G. Control of collagen production by human diploid lung fibroblasts. *J Biol Chem* **1980**, *255* (11), 5250-5260. From NLM Medline.
(39) Nanayakkara, A. K.; Vogel, P. D.; Wise, J. G. Prolonged inhibition of P-glycoprotein after exposure to chemotherapeutics increases cell mortality in multidrug resistant cultured cancer cells. *PLoS One* **2019**, *14* (6), e0217940. DOI: 10.1371/journal.pone.0217940.
(40) Daina, A.; Michielin, O.; Zoete, V. SwissADME: a free web tool to evaluate pharmacokinetics, drug-likeness and medicinal chemistry friendliness of small molecules. *Sci Rep* **2017**, *7*, 42717. DOI: 10.1038/srep42717.
(41) Doyle, L. A.; Yang, W.; Abruzzo, L. V.; Krogmann, T.; Gao, Y.; Rishi, A. K.; Ross, D. D. A multidrug resistance transporter from human MCF-7 breast cancer cells. *Proc Natl Acad Sci U S A* **1998**, *95* (26), 15665-15670. DOI: 10.1073/pnas.95.26.15665 From NLM Medline.
(42) Sarkadi, B.; Homolya, L.; Szakacs, G.; Varadi, A. Human multidrug resistance ABCB and ABCG transporters: participation in a chemoimmunity defense system. *Physiol Rev* **2006**, *86* (4), 1179-1236. DOI: 10.1152/physrev.00037.2005 From NLM Medline.
(43) Miyake, K.; Mickley, L.; Litman, T.; Zhan, Z.; Robey, R.; Cristensen, B.; Brangi, M.; Greenberger, L.; Dean, M.; Fojo, T.; et al. Molecular cloning of cDNAs which are highly overexpressed in mitoxantrone-resistant cells: demonstration of homology to ABC transport genes. *Cancer Res* **1999**, *59* (1), 8-13. From NLM Medline.
(44) Antoni, F.; Wifling, D.; Bernhardt, G. Water-soluble inhibitors of ABCG2 (BCRP) - A fragment-based and computational approach. *Eur J Med Chem* **2021**, *210*, 112958. DOI: 10.1016/j.ejmech.2020.112958.
(45) Taylor, N. M. I.; Manolaridis, I.; Jackson, S. M.; Kowal, J.; Stahlberg, H.; Locher, K. P. Structure of the human multidrug transporter ABCG2. *Nature* **2017**, *546* (7659), 504-509. DOI: 10.1038/nature22345 From NLM Medline.
(46) Jackson, S. M.; Manolaridis, I.; Kowal, J.; Zechner, M.; Taylor, N. M. I.; Bause, M.; Bauer, S.; Bartholomaeus, R.; Bernhardt, G.; Koenig, B.; et al. Structural basis of small-molecule inhibition of human multidrug transporter ABCG2. *Nat Struct Mol Biol* **2018**, *25* (4), 333-340. DOI: 10.1038/s41594-018-0049-1 From NLM Medline.
(47) Orlando, B. J.; Liao, M. ABCG2 transports anticancer drugs via a closed-to-open switch. *Nat Commun* **2020**, *11* (1), 2264. DOI: 10.1038/s41467-020-16155-2 From NLM Medline.

(48) Rasouli, A.; Yu, Q.; Dehghani-Ghahnaviyeh, S.; Wen, P. C.; Kowal, J.; Locher, K. P.; Tajkhorshid, E. Differential dynamics and direct interaction of bound ligands with lipids in multidrug transporter ABCG2. *Proc Natl Acad Sci U S A* **2023**, *120* (1), e2213437120. DOI: 10.1073/pnas.2213437120 From NLM Medline.
(49) Verma, V. A.; Wang, L.; Labadie, S. S.; Liang, J.; Sellers, B. D.; Wang, J.; Dong, L.; Wang, Q.; Zhang, S.; Xu, Z.; et al. Discovery of Inhibitors of the Lipopolysaccharide Transporter MsbA: From a Screening Hit to Potent Wild-Type Gram-Negative Activity. *J Med Chem* **2022**, *65* (5), 4085-4120. DOI: 10.1021/acs.jmedchem.1c01909 From NLM Medline.
(50) Administration, U. S. F. a. D. *Drug Development and Drug Interactions: Table of Substrates, Inhibitors and Inducers*. 2020. https://www.fda.gov/drugs/drug-interactions-labeling/drug-development-and-drug-interactions-table-substrates-inhibitors-and-inducers (accessed March 11, 2021).
(51) PubChem Compound Summary for CID 5284373, Cyclosporin A. https://pubchem.ncbi.nlm.nih.gov/compound/Ciclosporin. (accessed 14 August 2020).
(52) Moj, D.; Hanke, N.; Britz, H.; Frechen, S.; Kanacher, T.; Wendl, T.; Haefeli, W. E.; Lehr, T. Clarithromycin, Midazolam, and Digoxin: Application of PBPK Modeling to Gain New Insights into Drug-Drug Interactions and Co-medication Regimens. *AAPS J* **2017**, *19* (1), 298-312. DOI: 10.1208/s12248-016-0009-9.
(53) Wessler, J. D.; Grip, L. T.; Mendell, J.; Giugliano, R. P. The P-glycoprotein transport system and cardiovascular drugs. *J Am Coll Cardiol* **2013**, *61* (25), 2495-2502. DOI: 10.1016/j.jacc.2013.02.058.
(54) Amin, M. L. P-glycoprotein Inhibition for Optimal Drug Delivery. *Drug Target Insights* **2013**, *7*, 27-34. DOI: 10.4137/DTI.S12519.

SUPPLEMENTAL INFORMATION

Supplemental Table 1. Known P-gp Inhibitors and Predicted Chemical Properties. A non-exhaustive list of known P-gp inhibitors and their selected chemical properties [50, 51]. Clinical trial outcomes were adapted from [10, 11]. Compounds were evaluated using the SWISS-ADME server [40]. RO5: Rule of 5, MW: Molecular Weight, TPSA: Topological Polar Surface area, LogP: Average of 5 calculations of $LogP_{oct/wat}$, LogS: Average of 3 calculations to determine aqueous solubility – Insoluble, Poorly soluble (Poor), Moderately Soluble (Moderate), Soluble. "Predicted P-gp Substrate" - predicted by SWISS-ADME to be a transport substrate of P-gp. "Known P-gp Substrate" – In addition to being P-gp inhibitors, these molecules are: known transport substrates of P-gp, known non-transport substrates of P-gp, unknown whether it is a transport substrate of P-gp [52-54]. If the molecule is designated in a specific generation of P-gp inhibitors - First Generation P-gp inhibitors, Second generation P-gp inhibitors, Third generation P-gp inhibitors.

		Compound	MW (g/mol)	Clinical Trial Result	# RO5 Violations	TPSA (Å^2)	Log $P_{oct/wat}$	LogS	Predicted P-gp Substrate	P-gp Substrate?
Generation of P-gp Inhibitors	1st	Verapamil	455	Fail	0	64	4.45	Moderate	Yes	Yes
		Reserpine	609		2	118	3.52	Poor	Yes	No
		Cyclosporin A	1203	Fail	2	279	2.38	Poor	Yes	Yes
		Quinidine	324	Fail	0	46	2.81	Soluble	No	Yes
		Amiodarone	645	Fail	2	43	6.49	Poor	Yes	Yes
	2nd	Valspodar	1215	Fail	2	276	2.26	Poor	Yes	No
		Elacridar	564	Fail	1	93	4.93	Poor	No	Yes
		Dexverapamil	455	Fail	0	64	4.45	Moderate	Yes	No
	3rd	Tariquidar	647	Fail	1	111	5.2	Poor	No	Yes
		Zosuquidar	528	Fail	1	49	4.64	Poor	No	Yes

Supplemental Table 2. Normalized ratio of compound to internal standard using LC-MS/MS. DU145-TXR cells were exposed to 5 µM compound with or without 500 nM tariquidar (TQR) as described in [8]. Samples were prepared in triplicate and two or three independent trials were performed; data represent the mean ± one standard deviation (std. dev). In contrast to the methods used in [8], these LC-MS/MS trials measured the normalized ratio of analyte (i.e. compound) to the internal standard (i.e. unique performance of mass spectrometer on date of analysis); thus the data represent the relative quantification of compound per sample and explain the variability between independent trials (see Methods).

	- TQR	+ TQR	P	- TQR	+ TQR	P	- TQR	+ TQR	P
DAU	0.014 ± 0.001	0.216 ± 0.002	$< 1x10^{-6}$	0.017 ± 0.001	0.232 ± 0.016	$2x10^{-5}$			
60	0.231 ± 0.165	0.282 ± 0.010	0.6	0.250 ± 0.003	0.250 ± 0.003	> 1			
61	0.023 ± 0.002	0.076 ± 0.001	2×10^{-6}	0.016 ± 0.006	0.027 ± 0.011	0.2	0.021 ± 0.004	0.126 ± 0.010	0.0001
66	0.747 ± 0.096	0.833 ± 0.124	0.4	0.040 ± 0.001	0.036 ± 0.005	0.2	0.170 ± 0.039	0.140 ± 0.029	0.3
70	0.93 ± 0.15	0.93 ± 0.07	>1	0.56 ± 0.11	0.55 ± 0.15	0.9			
71	0.085 ± 0.013	0.067 ± 0.005	0.09	0.071 ± 0.009	0.091 ± 0.043	0.5			
74	0.014 ± 0.000	0.014 ± 0.001	> 1	0.028 ± 0.009	0.030 ± 0.005	0.8	11.51 ± 1.305	13.57 ± 0.248	0.05
78	0.001 ± 0.000	0.001 ± 0.000	--	0.001 ± 0.000	0.001 ± 0.000	--			
96	0.087 ± 0.009	0.092 ± 0.036	0.8	0.121 ± 0.005	0.163 ± 0.032	0.09			
97	0.07 ± 0.02	0.08 ± 0.03	0.7	0.10 ± 0.02	0.10 ± 0.02	> 1			
101	11.86 ± 1.16	12.03 ± 2.45	0.9	21.17 ± 3.59	22.88 ± 2.92	0.6			
103	5.13 ± 0.6	5.61 ± 1.34	0.6	2.63 ± 0.52	3.75 ± 0.34	0.04	3.21 ± 0.23	3.73 ± 0.15	0.03
111	0.012 ± 0.002	0.013 ± 0.004	0.7	0.011 ± 0.002	0.013 ± 0.001	0.2			
122	0.049 ± 0.005	0.146 ± 0.018	0.0008	0.058 ± 0.018	0.209 ± 0.014	0.0003			
124	0.006 ± 0.001	0.061 ± 0.011	0.001	0.007 ± 0.002	0.055 ± 0.009	0.0008			

Supplemental Table 3. Fold Accumulation of Daunorubicin fluorescence in DU145-TXR cells. Here we show the fold fluorescence of the P-gp substrate Daunorubicin (DAU) in the presence or absence of experimental compounds or known P-gp modulators. Cells were treated with 10 µM compound in the presence or absence of 10 µM DAU, after which cells were washed and lysed; the resultant DAU fluorescence was measured on the Cytation 5 (excitation/emission 488 nm / 575 nm). The resultant DAU fluorescence is expressed as a fold change relative to the fluorescence of DU145-TXR cells treated with DAU alone. The P-gp inhibitors VPL and TQR were included as positive controls for P-gp inhibition, and compound 59 was included as a negative control for P-gp inhibition. N = 9, with three samples per trial, three trials. Statistical significance determined using GraphPad Prism, Student's T test of the mean. Significance was determined using a Student's T test of the mean; P > 0.05 = N.S., P < 0.05 = *, P < 0.01 = **, P < 0.001 = ***, P < 0.0001 = ****.

	Fold Δ	**P Value**	**Significance**
DAU Alone	1.0 ± 0.3		
DAU + 59	0.9 ± 0.2	P = 0.48	N.S.
DAU + 70	1.4 ± 0.3	P = 0.01	*
DAU + 78	0.75 ± 0.1	P = 0.03	*
DAU + 96	2.4 ± 0.4	P < 0.0001	****
DAU + 97	1.9 ± 0.4	P < 0.0001	****
DAU + 101	2.3 ± 0.4	P < 0.0001	****
DAU + 103	4.5 ± 2.6	P = 0.001	**
DAU + 111	1.0 ± 0.2	P = 0.75	N.S.
DAU + VPL	6.3 ± 1.0	P < 0.0001	****
DAU + TQR	6.5 ± 1.6	P < 0.0001	****

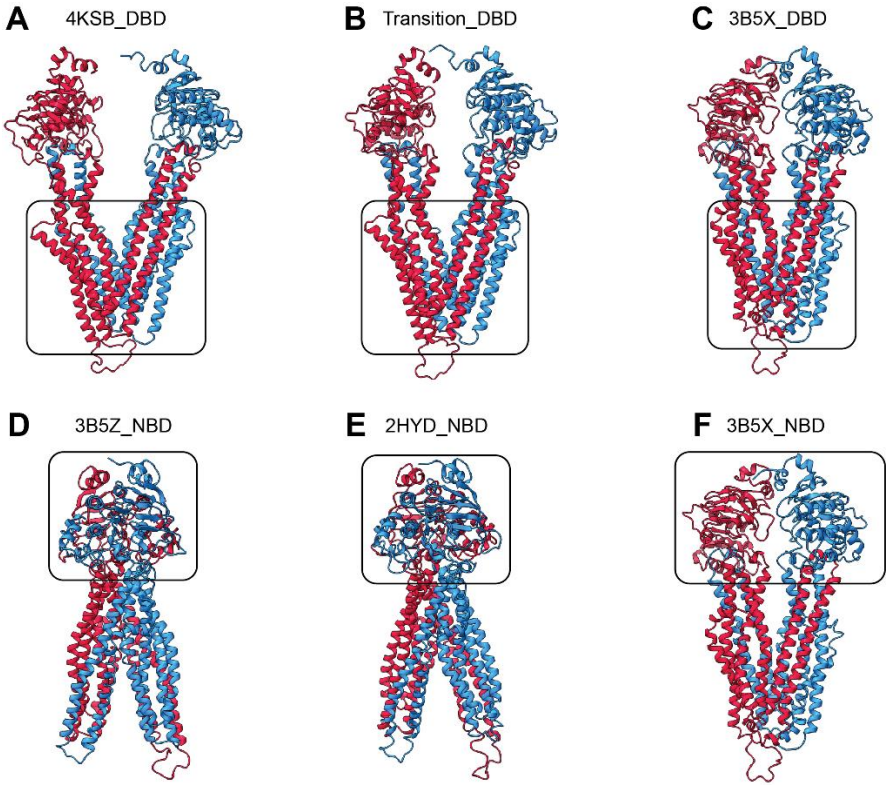

Supplemental Figure 1. Target structures for docking studies. **Panel 1:** A. 4KSB_DBD, B. Transition_DBD, C. 3B5X_DBD, D. 3B5Z_NBD_1 and 3B5Z_NBD_2, E. 2HYD_NBD_1 and 2HYD_NBD_2, F. 3B5X_NBD. The NBD of the Transition structure in B was also sampled. NBD dock boxes for the 2HYD and 3B5Z structures were designed to sample each NBD individually. A-F are human P-gp structures. Boxes correspond to the region targeted using AutoDock Vina with an exhaustiveness of 128.

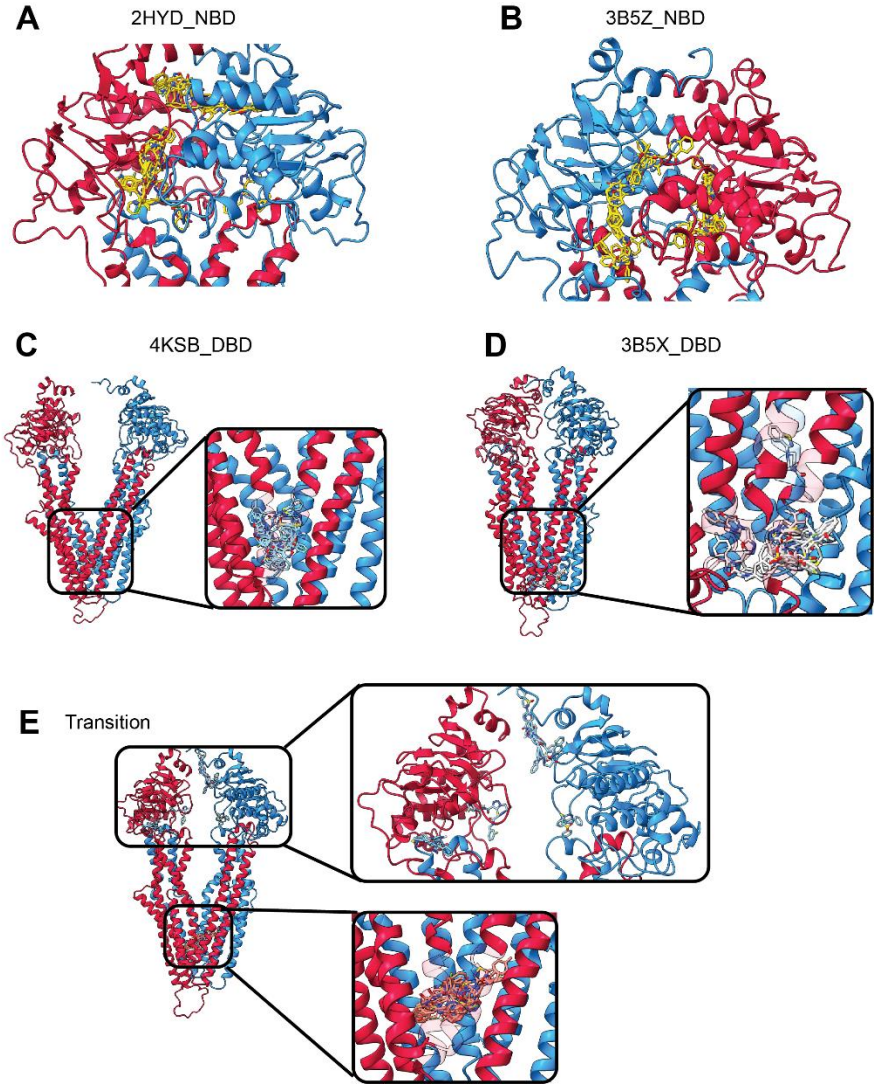

Supplemental Figure 2. Ligand docking locations to each P-gp structure. The docking positions of the top hits to the NBDs of **A)** 2HYD and **B)** 3B5Z were mostly located within the ATP-binding site, with the exception of a few positions above the ATP-binding site in 2HYD. The docking positions of top hits to the DBDs of **C)** 4KSB and **D)** 3B5X were near the middle or the bottom of the drug binding region, respectively. Ligands were docked to both the **E, top box)** NBDs and **E, bottom box)** DBDs of the "Transition" structure, which was generated from MD simulation trajectories that transitioned the protein from the 4KSB to the 3B5X conformation. It is notable that several hits were predicted to bind near the ATP-binding sites, even though, when the NBDs are disengaged, the catalytic configuration for ATP hydrolysis is incomplete.

Supplemental Table 4. Ratio of estimated affinities ($K_D^{estimate}$) for the top hits. Ratios are calculated as the estimated DBD affinity (K_D^{DBD}) divided by the estimated NBD affinity (K_D^{NBD}). Ratios are listed by compound, and then organized by receptor structure. Three DBD docking boxes and five NBD boxes were used (Supplemental Figure 1). Each NBD of the 2HYD and 3B5Z structures was given its own docking box, hence the labels "nbd_1" and "nbd_2". Molecules with a high ratio of DBD/NBD affinities are the most desirable, as this indicates that the $K_D^{estimate}$ to the DBDs is much larger (and thus lower affinity) than the $K_D^{estimate}$ to the NBDs.

	4KSB DBD / NBD				
SMU ID	2hyd_nbd_1	2hyd_nbd_2	3b5z_nbd_1	3b5z_nbd_2	transition_nbd
70	3.3	57.3	3.9	3.3	6.4
78	1.0	1.0	1.2	0.2	0.4
96	0.3	0.4	0.0	0.0	0.0
97	2.8	0.7	1.0	0.1	0.1
101	2.0	40.9	5.4	2.8	2.8
103	--	12.6	3.9	0.4	1.7
111	0.7	0.5	0.7	0.1	0.7
122	14.9	7.6	17.6	3.9	2.3
124	7.6	57.3	1.7	5.4	1.2
	3B5X DBD / NBD				
SMU ID	2hyd_nbd_1	2hyd_nbd_2	3b5z_nbd_1	3b5z_nbd_2	transition_nbd
70	6.4	112.6	7.6	6.4	12.6
78	3.9	3.9	4.6	0.8	1.4
96	3.9	6.4	0.2	0.1	0.1
97	6.4	1.7	2.3	0.3	0.2
101	2.3	48.4	6.4	3.3	3.3
103	--	14.9	4.6	0.5	2.0
111	6.4	4.6	6.4	1.2	6.4
122	7.6	3.9	9.0	2.0	1.2
124	9.0	67.9	2.0	6.4	1.4
	Transition DBD / NBD				
SMU ID	2hyd_nbd_1	2hyd_nbd_2	3b5z_nbd_1	3b5z_nbd_2	transition_nbd
70	0.8	14.9	1.0	0.8	1.7
78	1.7	1.7	2.0	0.4	0.6
96	4.6	7.6	0.3	0.2	0.1
97	2.3	0.6	0.8	0.1	0.1
101	1.2	24.7	3.3	1.7	1.7
103	--	1.4	0.4	0.0	0.2
111	0.8	0.6	0.8	0.2	0.8
122	1.4	0.7	1.7	0.4	0.2
124	4.6	7.6	0.3	0.2	0.1

Supplemental Table 5. Alternative identifiers for molecules identified in this study. ZINC IDs are shown if available. Molecular structures are translated into SMILES, and the corresponding InChl keys are provided as well.

#	SMILES	InChl Key	ZINC
59	Cn1cnnc1SCc1c(nnn1-c1nonc1N)C(O)=O	HRULNCRRUBFEHC-UHFFFAOYSA-N	130193
60	Nc1nonc1-n1nnc(C(=O)N\N=C\c2c3ccccc3cc3ccccc23)c1COc1ccc(F)cc1	IUYYNPMYIXKERT-AMVVHIIESA-N	2394477
61	CCN1CCN(Cc2c(nnn2-c2nonc2N)C(=O)N\N=C2\C(=O)N(C)c3ccccc23)CC1	AIPNQMGXBPYYIH-XQNSMLJCSA-N	22874636
66	O=C(N1CCN(CC1)S(=O)(=O)c1cccc2nonc12)c1cc2ccccc2[nH]1	ANFMLYJTRAARTN-UHFFFAOYSA-N	13727116
70	O=C(N1CCN(CC1)c1nsc2ccccc12)c1nc(no1)-c1ccc2cc[nH]c2c1	WFCVBKDGPGPBHN-UHFFFAOYSA-N	12389647
71	COc1ccc(OC)c(NC(=O)c2nnn(c2C)-c2ccc3noc(-c4ccccc4)c3c2)c1	XLBUSWFGBQBUHE-UHFFFAOYSA-N	12274469
78	Cc1onc(c1-c1nnc(Cn2cnc3c4ccccc4oc3c2=O)o1)-c1ccccc1	RZONHOSTPSUOJP-UHFFFAOYSA-N	31744412
79	Cc1cccc(c1)C1Cc2c(cnn2-c2nc3ccccc3[nH]2)C(=O)C1	JBULLGGIBFROGV-UHFFFAOYSA-N	9421694,9421695
89	NS(=O)(=O)c1cccc(NC(=O)CSc2nnnn2C2CC2)c1	BFXWBYBENJOJND-UHFFFAOYSA-N	12808366
96	O=S(=O)(CCSc1nnc(-c2ccccc2)c2ccccc12)c1ccccc1	KHUMXFJGOTYFBR-UHFFFAOYSA-N	84559953
97	OC(Cn1c(CS(=O)(=O)c2ccccc2)nc2ccccc12)c1ccc(Cl)cc1	VJMMFJLYEGJEAG-UHFFFAOYSA-N	
101	COc1cccc(c1)N1CCN(CC1)c1ccc2nnc(CCC(=O)Nc3ccc(F)c(F)c3)n2n1	AWFWASCTYWHYJR-UHFFFAOYSA-N	9118852
103	Cc1ccc(cc1)-c1noc(n1)-c1cn(Cc2ccc(NS(=O)(=O)c3ccccc3F)cc2)cn1	LZOCKGYCAZNWJT-UHFFFAOYSA-N	32974765
111	Cc1onc(c1-c1nnc(Cn2cnc3ccccc3c2=O)o1)-c1ccccc1	BTXVFIOVOXQJSY-UHFFFAOYSA-N	12922226
122	Fc1cccc(CNC(=O)c2nnn3CCn4nnc(C(=O)NCc5cccc(F)c5)c4Sc23)c1	WZQVWCJCOLIHHH-UHFFFAOYSA-N	36489963
124	O=C(N1CCN(CC1)c1nsc2ccccc12)c1nc(no1)-c1ccccn1	NZHVFOMJJPILIA-UHFFFAOYSA-N	12408039

Supplemental Table 6. **Pre-screening of compounds 56 – 98 against DU145-TXR cells with resazurin assays**. DU145-TXR cells were incubated with 15 µM compound with or without 500nM PTX for 48 hrs; survival was subsequently determined with the Resazurin viability assay [27]. Data represent the mean of two separate experiments performed in triplicate, and shows viability of cells treated with 15 µM compound alone, 15 µM compound and 500 nM PTX, and the difference between survivability measurements of each treatment. Percent resensitization is defined as the percent change in viability between cells treated with compound and PTX, versus cells treated with PTX alone. In some instances, the assay reported an increase in viability with compound + PTX, and no percent sensitization is reported. 'Follow-up Testing' compounds were re-assessed with MTT assays (Figure 1). Compounds 59 and 89 (*, 'Follow-up Testing') were used as negative controls in follow-up MTT assays to test for consistency of results, e.g. to confirm that molecules eliminated in Rezasurin assays were justifiably eliminated from later screening with MTT assays. Tariquidar was included as a positive control for P-gp inhibition.

	15 µM compound alone	15 µM compound + 500 nM PTX	Change in viability	Percent (%) sensitization	Followup testing?
56	96.3	96.9	+0.6		
57	70.3	64.8	5.5	7.8	
58	99.9	97.8	2.1	2.1	
59	101.1	100.8	0.3	0.3	*
60	88.0	47.0	41	46.6	Yes
61	98.8	53.1	45.7	46.3	Yes
62	100.6	99.2	1.4	1.4	
63	97.6	100.8	+3.2		
64	94.7	98.2	+3.5		
65	94.8	99.1	+4.3		
66	98.3	46.0	52.3	53.2	Yes
67	89.8	92.6	+2.8		
68	86.6	54.4	32.2	37.2	Yes
69	106.3	101.7	4.6	4.3	
70	99.2	61.6	37.6	37.9	Yes
71	93.0	38.2	54.8	58.9	Yes
72	95.3	75.2	20.1	21.1	
73	101.2	97.7	3.5	3.5	
74	73.3	45.9	27.4	37.4	Yes
75	99.8	97.6	2.2	2.2	
76	103.5	100.5	3.0	2.9	
77	95.7	93.5	2.2	2.3	
78	95.2	14.5	80.7	84.8	Yes
79	89.9	51.2	38.7	43.0	Yes

80	95.4	95.1	0.3	0.3	
81	77.4	74.8	2.6	3.4	
82	97.7	96.7	1.0	1.0	
83	98.0	79.0	19.0	19.4	
84	101.9	105.6	+3.7		
85	99.5	100.9	+1.4		
86	97.3	96.8	0.5	0.5	
87	53.1	53.4	+0.3		
88	94.1	90.2	3.9	4.1	
89	93.7	92.9	0.8	0.9	*
90	97.4	95.5	1.9	2.0	
91	99.6	94.0	5.6	5.6	
92	99.9	98.6	1.3	1.3	
93	100.5	97.7	2.8	2.8	
94	98.8	96.3	2.5	2.5	
95	95.6	77.8	17.8	18.6	
96	89.4	16.1	73.3	82.0	Yes
97	102.2	63.6	38.6	37.8	Yes
98	97.4	80.1	17.3	17.8	
TQR	75.2	9.1	66.2	87.9	